iScience

CellPress

Article

Functional Heterogeneity of Mouse Prostate Stromal Cells Revealed by Single-Cell RNA-Seq

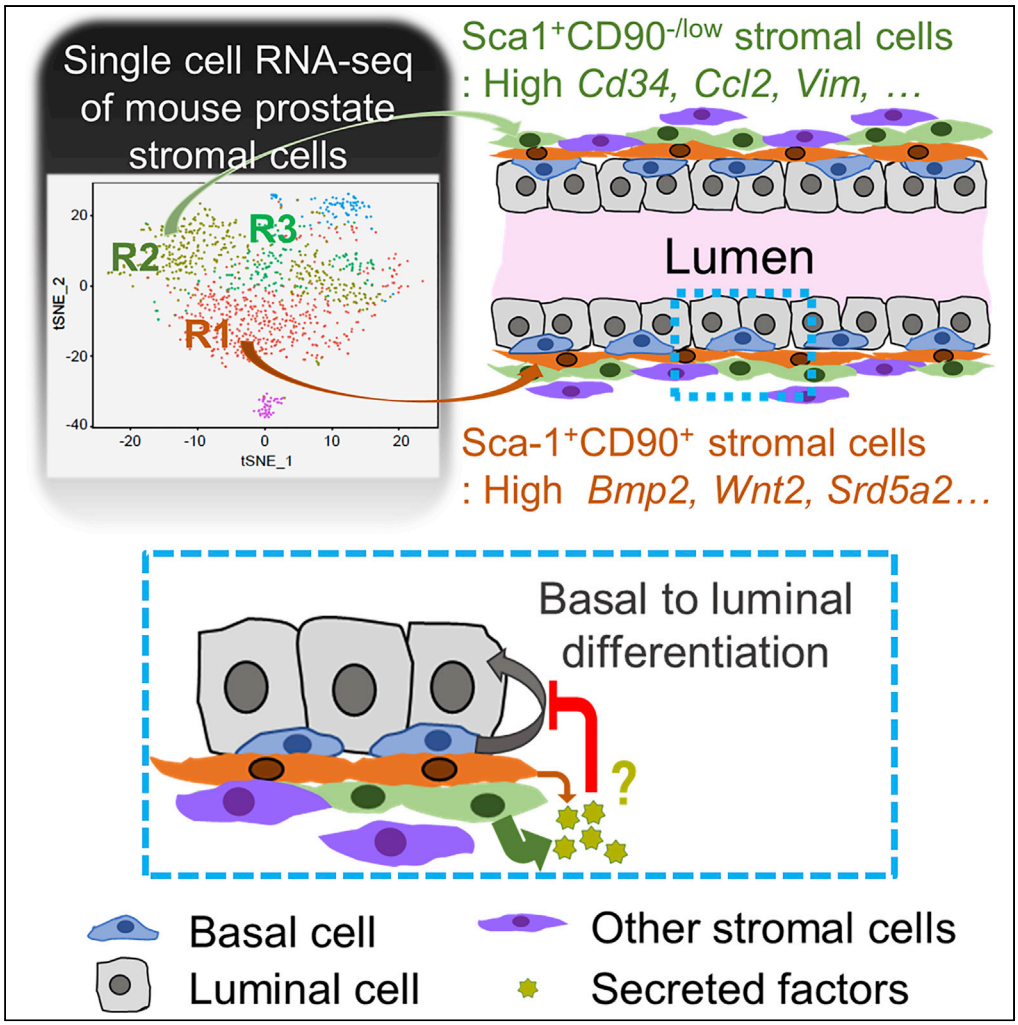

Oh-Joon Kwon, Yiqun Zhang, Yumei Li, ..., Rui Chen, Chad J. Creighton, Li Xin

xin18@uw.edu

HIGHLIGHTS

scRNA-seq reveals three distinct mouse prostate stromal cell populations

Sca-1^{+}CD90^{+} cells produce growth factors mediating developmental process

Sca-1^{+}CD90$^{-/low}$ cells express genes mediating immune response and tissue repair

Sca-1^{+}CD90$^{-/low}$ cells robustly suppress bipotent differentiation of basal cells

DATA AND SOFTWARE AVAILABILITY

GSE119988

Kwon et al., iScience *13*, 328–338
March 29, 2019
https://doi.org/10.1016/j.isci.2019.02.032

iScience

CellPress

Article

Functional Heterogeneity of Mouse Prostate Stromal Cells Revealed by Single-Cell RNA-Seq

Oh-Joon Kwon,[1,6] Yiqun Zhang,[2] Yumei Li,[3] Xing Wei,[1,4,6] Li Zhang,[6] Rui Chen,[3] Chad J. Creighton,[2,5] and Li Xin[1,2,6,7,8,*]

SUMMARY

We perform a single-cell RNA sequencing analysis to investigate the phenotypic and functional heterogeneity of the adult mouse prostate stromal cells. Our analysis identifies three major cell populations representing the smooth muscle cells and two types of fibroblast cells enriched by Sca-1 and CD90. The Sca-1^{+}CD90^{+} fibroblast cells are in direct contact with the epithelial cells and express growth factors and genes associated with cell motility, developmental process, and androgen biosynthesis. This suggests that they may regulate epithelial cell survival and growth. The Sca-1^{+}CD90$^{-/low}$ myofibroblast-like cells highly express genes associated with the extracellular matrix and cytokine-mediated signaling pathways, indicating a role in tissue repair and immune responses. The Sca-1^{+}CD90$^{-/low}$ cells significantly suppress the capacity of the basal cells for bipotent differentiation in the prostate organoid assay. Collectively, we identify the surface markers enabling physical separation of stromal subpopulations and generate the gene expression profiles implying their cellular functions.

INTRODUCTION

The prostate is an organ that develops from the embryonic urogenital sinus under the regulation of androgens (Marker et al., 2003). Besides the endoderm-derived epithelial cells, there are many other types of cells of different embryonic origins in the prostate, such as the stromal cells, immune cells, endothelial cells, nerve cells, and adipocytes. The term *prostate stromal cells* is vague, but generally refers to the non-hematopoietic and non-epithelial fibroblast cells. Stromal-epithelial interaction has been demonstrated to play an important role in the development and homeostasis of the prostate as well as in the initiation and progression of the prostate-related diseases including prostate cancer and benign prostatic hyperplasia (Barron and Rowley, 2012; Brennen et al., 2013; Cunha and Ricke, 2011; Risbridger and Taylor, 2008; Strand et al., 2017).

During the past few decades, much progress has been made in understanding the lineage hierarchy of the prostate epithelial cells, especially that in the mouse (Lawson and Witte, 2007; Shibata and Shen, 2013; Xin, 2013). In contrast, our understanding of the stromal lineages lags. Stromal cells are abundant in the human prostate but are relatively scarce in the mouse prostate. It is well accepted that the prostate stromal cells consist of distinct subpopulations with different functions and cellular origins. Functionally, the prostate stromal cells consist of smooth muscle cells and fibroblasts. The smooth muscle cells carry the contractile function. In the literature, mouse prostate smooth muscle cells are often roughly identified as bands of cells encapsulating prostatic epithelial glands based on the expression of α-smooth muscle actin. Fibroblast cells are referred to as the cells expressing vimentin and are often found in the interglandular space. Fibroblasts per se are also heterogeneous depending on their activation states and play important roles in immune surveillance and tissue repair (Kalluri, 2016; Ohlund et al., 2014). Fibroblasts are thought to be capable of differentiating into myofibroblasts and then to smooth muscle cells in a reversible manner (Barron and Rowley, 2012). A recent study classified the mouse prostate stroma into four compartments based on the expression of α-smooth muscle actin and CD34, but the functional relevance of this classification is unknown (Peng et al., 2013). In addition, how the homeostasis of the prostate stromal cells is maintained remains unclear. Several studies demonstrated the existence of resident and infiltrated stromal cells in the prostate that possess the multipotent stem cell activity (Brennen et al., 2016; Kim et al., 2014; Lin et al., 2007). However, a lineage tracing study by Peng et al. suggested that distinct stromal cell subpopulations are replenished independently (Peng et al., 2013).

Source of support: NIDDK.

[1]Department of Molecular and Cellular Biology, Baylor College of Medicine, Houston, TX, USA

[2]Dan L. Duncan Comprehensive Cancer Center, Baylor College of Medicine, Houston, TX, USA

[3]Department of Molecular and Human Genetics, Baylor College of Medicine, Houston, TX, USA

[4]Graduate Program in Integrative Molecular and Biomedical Sciences, Baylor College of Medicine, Houston, TX, USA

[5]Department of Medicine, Baylor College of Medicine, Houston, TX, USA

[6]Department of Urology, University of Washington, 850 Republican Street, Seattle, WA 98109, USA

[7]Institute of Stem Cell and Regenerative Medicine, University of Washington, Seattle, WA, USA

[8]Lead Contact

*Correspondence: xin18@uw.edu

https://doi.org/10.1016/j.isci.2019.02.032

Despite these findings, our understanding of the prostate stromal cells is quite limited. There is a lack of the marker that can definitively define individual stromal cell subpopulations. Fibroblast-specific protein 1, actin alpha 2, and vimentin are frequently used markers for the prostate stromal cells. However, these markers cannot distinguish different stromal cell lineages under physiological and pathological conditions and are also not specific to the stromal cells. In addition, they are all intracellular proteins. Therefore it is technically infeasible to use these antigens to investigate the heterogeneity of the stromal cells, separate different stromal cell lineages, and uncover novel information regarding stromal cell biology and function.

Recent breakthrough in global analysis of transcriptomes at the single-cell level has made it possible to study cellular lineage heterogeneity and relationship (Papalexi and Satija, 2017; Treutlein et al., 2014; Wollny et al., 2016). In this study, we perform single-cell RNA sequencing (scRNA-seq) analysis of adult mouse prostate stromal cells. Our study indicates that there are three major cell populations in the prostate stroma that roughly represent smooth muscle cells and two types of fibroblast cells. Our study identifies novel surface markers that enable physical separation of the different cell fractions and generate gene expression profiles that not only corroborate known cellular roles but also imply previously unknown functions of these cell lineages.

RESULTS

ScRNA-Seq Reveals Distinctive Subpopulations in Adult Mouse Prostate Stromal Cells

To dissect the stromal cell heterogeneity in the adult mouse prostates, we performed scRNA-seq analysis of individual adult mouse prostate stromal cells. Prostate stromal cells were isolated by fluorescence-activated cell sorting (FACS) from 8- to 10-week-old C57BL/6 mice based on their surface antigen expression profile ($Lin^-CD24^-CD49f^-$) (Figure S1A) (Xin et al., 2005). We employed the iCell8 Single-Cell System (Takara Bio) for single-cell capture to achieve an intermediate in-depth expression profiling of single prostate stromal cells. Combined with Illumina sequencing, we were able to assign on the order of 78 million reads and detect up to 3,967 genes per cell. We analyzed profiles from 1,159 single stromal cells that passed strict quality control thresholds (Transparent Methods) and used the Seurat 2.0 clustering algorithm to identify robust clusters of cells within the data. Using these methods, we identified five major clusters of cell populations (Figure 1A). To determine the identities and functions of each subpopulation, we compiled the top 200 genes that could be specifically associated with each subgroup (Figure 1B) and performed Gene Ontology (GO) (Figure 1C) and network pathway analyses (Figure S1B) for each subgroup based on differential genes. Figure 1D shows some representative genes of biological interest for each subpopulation.

Three subpopulations (R1–R3) constitute most of the FACS-isolated single stromal cells, whereas the R4 and R5 subpopulations represent 4% and 7% of the total cells, respectively. The R5 subpopulation likely represents the luminal epithelial cell contamination because it highly expresses the luminal-cell-associated genes such as *Krt8*, *Krt18*, *Cdh1*, and *Pbsn* (Figure 1D). Gene ontology analysis shows that the R4 cells express genes associated with DNA packaging, nucleosome assembly, and organization (Figure 1C). However, the identity and function of this small cell population remain unclear based on the top expressed genes and the GO analysis. Therefore we focused on the characterization of the R1–R3 subpopulations in this study.

The R1 subpopulation (42% of the total cells) highly expresses a fibroblast cell marker *Thy-1* (CD90) but expresses a relatively lower level of another fibroblast marker *Vimentin* (Figure 1D). GO analysis shows that these cells express genes associated with extracellular matrix, anatomical structure morphogenesis, cell motility, developmental process, and Wnt signaling (Figure 1C), including *Mmp2*, *Bmp2*, *Bmp7*, *Hoxd13*, *Yap1*, *Runx2*, and Wnt signaling components (*Wnt2*, *Fzd1*, *Tcf4*, *Lef1*, *Sfrp2*, and *Wif1*) (Figure 1D). This indicates that this cell population mediates signaling that regulates prostate morphogenesis. In addition, *Srd5a2*, an essential enzyme for dihydrotestosterone (DHT) production is also highly expressed in this cell population (Figure 1D), which suggests that these cells play a critical role in the prostatic intracrine androgen biosynthesis (Wang et al., 2017).

The R2 subpopulation (34% of the total cells) highly expresses *S100a4* (*Fsp1*), *Ddr2*, *Fn1*, and *Igf1* (Figure 1D). It also highly expresses *Cd34* and *Ly6* family members (Ly6a, Ly6c1, and Ly6c2), but expresses a relatively lower level of *Cd200*. The R2 subpopulation expresses many genes associated with the extracellular matrix and exosome, cytokine- and chemokine-mediated signaling pathways, and complement activation (Figure 1C), including many cytokines, chemokines, and complement components such as *Ccl2*,

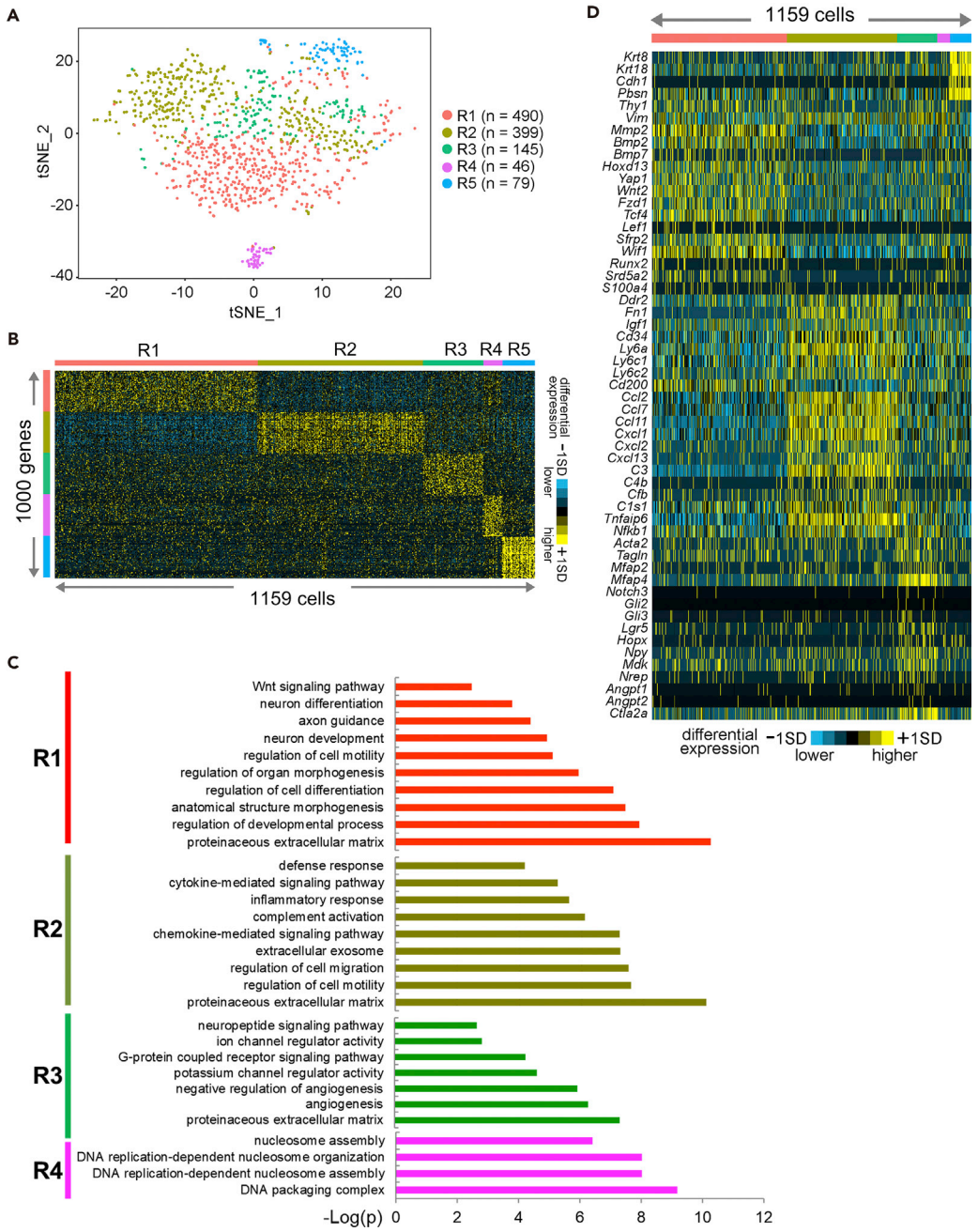

Figure 1. scRNA-seq Reveals Distinctive Subpopulations on Prostate Stromal Cells

(A) Multidimensional scaling plot of scRNA-seq identifies five clusters of populations (R1–R5).

(B) Heatmap showing clustering with top 200 highly expressed genes within each group.

(C) Gene Ontology analysis of subpopulations of prostate stromal cells.

(D) Heatmap of selected genes differentially expressed among prostate stromal subpopulations.

See also Figure S1.

Ccl7, *Ccl11*, *Cxcl1*, *Cxcl2*, and *C3* (Figure 1D). Collectively, these observations indicate that the R2 subpopulation may play a role in defense and immune responses and tissue repair.

Cells in the R3 cluster (12.5% of the total cells) highly express *Acta2*, *Tagln*, *Mfap2*, and *Mfap4*, suggestive of a smooth muscle cell phenotype (Figure 1D). In addition, *Notch3*, *Gli2*, *Gli3*, *Rspo3*, and two stem cell-associated

markers, *Lgr5* and *Hopx*, are also highly expressed in this cell population. GO analysis reveals that the genes associated with the potassium channel regulator activity (*Cav1*, *Kcnip1*) are enriched among the top 200 genes of the R3 subgroup (Figure 1C). This is consistent with the ion-channel-mediated contractile function of the smooth muscle cells. Interestingly, these cells also expressed various neuropeptide genes (*Npy*, *Mdk*, and *Nrep*) and regulators of angiogenesis (*Angpt1*, *Angpt2*, and *Ctla2a*) (Figure 1C), suggesting the existence of cross talk between these cells with the nerves and endothelial cells.

Isolation of Distinctive Mouse Prostatic Stromal Cell Populations Based on Surface Expression Profiles

We sought to use surface antigens identified in the scRNA-seq analysis to separate the prostate stromal cells into functionally distinct subpopulations. According to the scRNA-seq analysis, *Cd90* and *Cd200* are highly expressed in the R1 cells, whereas *Sca-1* and *Cd34* are highly expressed by the R2 cells. FACS analysis revealed that all $CD90^+$ cells are $CD200^+$, whereas most $CD34^+$ (all $CD34^{high}$) cells are $Sca\text{-}1^+$ (Figure S1C). We therefore attempted to use CD200 and Sca-1 to further fractionate stromal cells. Surprisingly, contrary to the inverse correlation between the expression of CD200 and Sca-1 shown in the scRNA-seq analysis, the two antigens costained predominantly in the FACS analysis (Figure S1D). This is probably because one of the markers is expressed at a very wide range. We therefore used CD90 instead, in combination with Sca-1, to further fractionate prostate stromal cells.

As shown in Figure 2A, Sca-1 and CD90 separate the $Lin^-CD24^-CD49f^-$ stromal cells into four populations (S1, $Sca\text{-}1^+CD90^+$, 36.7%; S2, $Sca\text{-}1^+CD90^{-/low}$, 21.6%; S3, $Sca\text{-}1^-CD90^+$, 6.6%; S4, $Sca\text{-}1^-CD90^-$, 35.1%). Immunostaining of cytospin preparations revealed that the S4 population was mainly composed of cell debris (data not shown). To determine the identities of the remaining three cell populations, we FACS-isolated individual cell populations, extracted RNAs, and performed qRT-PCR analysis of the genes associated with the three subpopulations (R1–R3) identified by the scRNA-seq analysis (Figure 1D). Figures 2B and 2C show that the S1 and S2 fractions highly express representative genes enriched in the R1 and R2 populations, respectively. However, among the genes enriched in the R3 population, only *Notch3* and *Cav1* were highly expressed in the S3 cell population, whereas other genes were mostly expressed in the S2 cells, suggesting that the R3 cell population was not efficiently separated from the R2 cells using this combination of surface antigens (Figure S2A). Of note, S2 cells also highly express *Acta2* (Figure S2A). Considering that many factors expressed by myofibroblasts are highly expressed in the S2 cells, such as *Acta2*, *Fn1*, and inflammatory cytokines (Sun et al., 2016), it is naturally to reason that the R2/S2 cells represent myofibroblast cells.

We also investigated the expression levels of several major hormone receptors in the three cell populations (Figure 2D). Estrogen receptor α (*Esr1*) and progesterone receptor (*Pr*) are expressed at a relatively higher level in the S1 and S3 cells, whereas glucocorticoid receptor (*Gr*) is highly expressed in the S2 cells. The androgen receptor is expressed in all the three subpopulations at a similar level. The proliferative index of the S1 cells is relatively higher than those of the S2 and S3 cells based on the flow cytometric analysis of bromodeoxyuridine incorporation (Figure 2E).

The molecular and phenotypic profiles of individual stromal subpopulations are quite stable. For example, after FACS-isolated S1 and S2 cells were cultured and expanded in Petri dish separately, they still expressed their respective representative genes differentially (Figure S2B), although the expression levels of these genes decreased significantly in the cultured cells than in freshly isolated cells (Figures 2B and 2C). In addition, when these cells were cultured *in vitro* in Matrigel under the condition of a prostate organoid culture (Karthaus et al., 2014) they retained their respective surface marker expression profiles (Figures S2C and S2D). These observations suggest that the two fibroblast subpopulations have undergone a strict lineage specification and do not display lineage plasticity at least under these two *in vitro* culture conditions.

Anatomic Localization and Hormonal Regulation of Different Stromal Cell Populations

We then investigated whether the three different stromal cell populations separated by Sca-1 and CD90 are equally distributed among different mouse prostatic lobes. Figures 3A and 3B show that the $Sca\text{-}1^+CD90^+$ S1 population is rare in the ventral prostate but is most abundant in the anterior lobe. Immunostaining corroborates that Sca-1 is expressed in the stromal cells in all different lobes, but CD90 is barely detectable in the ventral prostate stromal cells (Figures 3C and S3A). Owing to the restriction of the source species of the antibodies, we were not able to perform coimmunostaining of Sca-1 and CD90. Instead, we performed

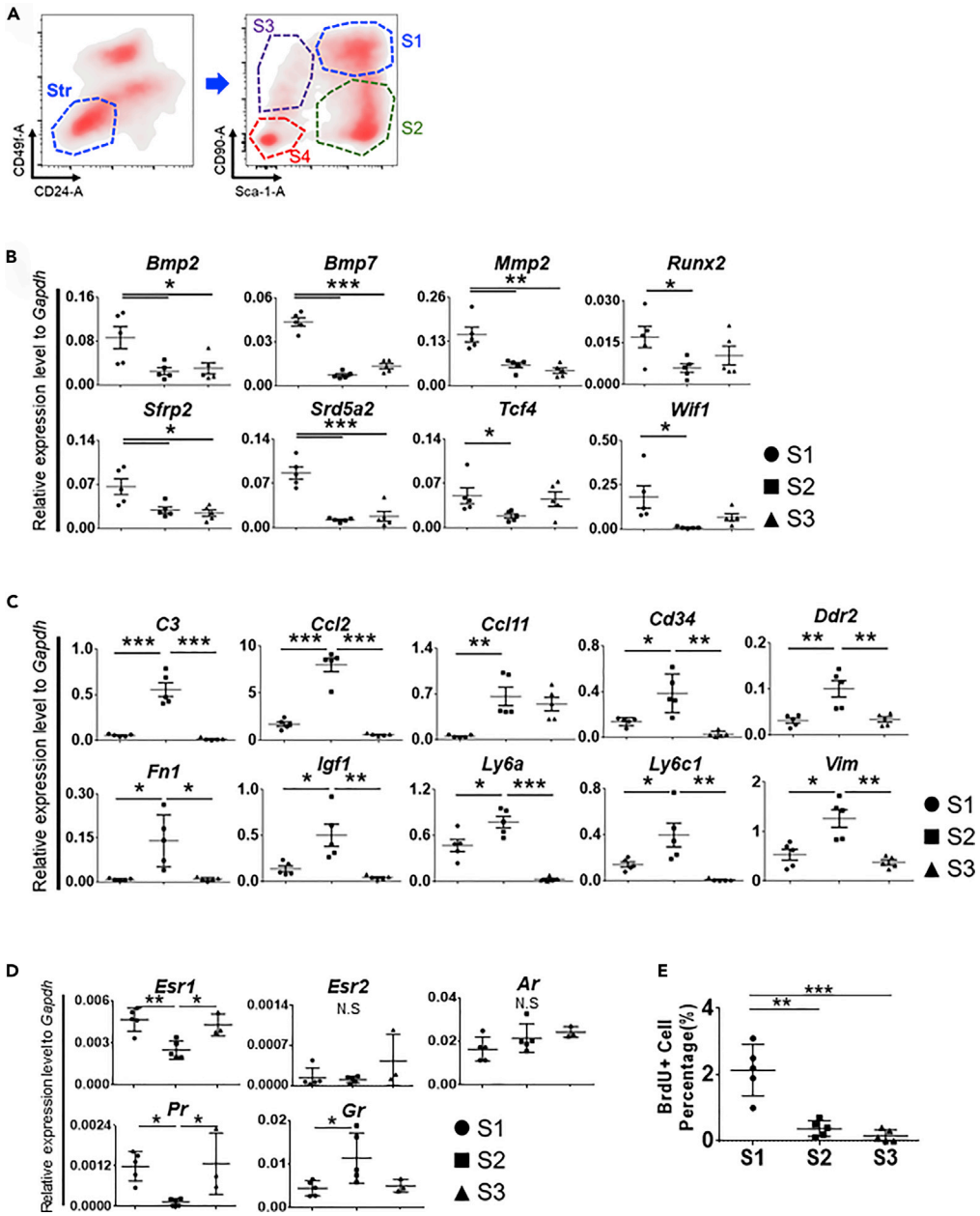

Figure 2. Sca-1 and CD 90 Fractionates Prostate Stromal Cells

(A) FACS plot shows that Sca-1 and CD90 fractionate four distinct subpopulations on prostate stromal cells.

(B) qRT-PCR analysis of R1-cell-associated genes in FACS-sorted prostate stromal subpopulations. Results show means ± SEM from five independent experiments. *p < 0.05, **p < 0.01, ***p < 0.001.

(C) qRT-PCR analysis of R2-cell-associated genes. Dot plot shows means ± SEM of relative expression to *Gapdh* (N = 5 each). *p < 0.05, **p < 0.01, ***p < 0.001.

(D) qRT-PCR analysis of hormone receptors. Dot plot shows means ± SEM of relative expression to *Gapdh* (N = 5 for S1 and S2 and N = 3 for S3). *p < 0.05, **p < 0.01.

(E) Dot plot shows means ± SEM of percentage of $BrdU^+$ cells in stromal subpopulations by flow cytometric analysis. **p < 0.01, ***p < 0.001. BrdU, bromodeoxyuridine.

See also Figure S2.

coimmunostaining of CD34 and CD90. Consistent with the scRNA-seq and FACS analyses (Figures 1D and S1C), CD34 staining surrounds the keratin 14-expressing basal cells and overlapped significantly with Sca-1 staining in stromal cells (middle and bottom panels, Figures 3C, S3B, and S3C). In contrast, CD90 and CD34

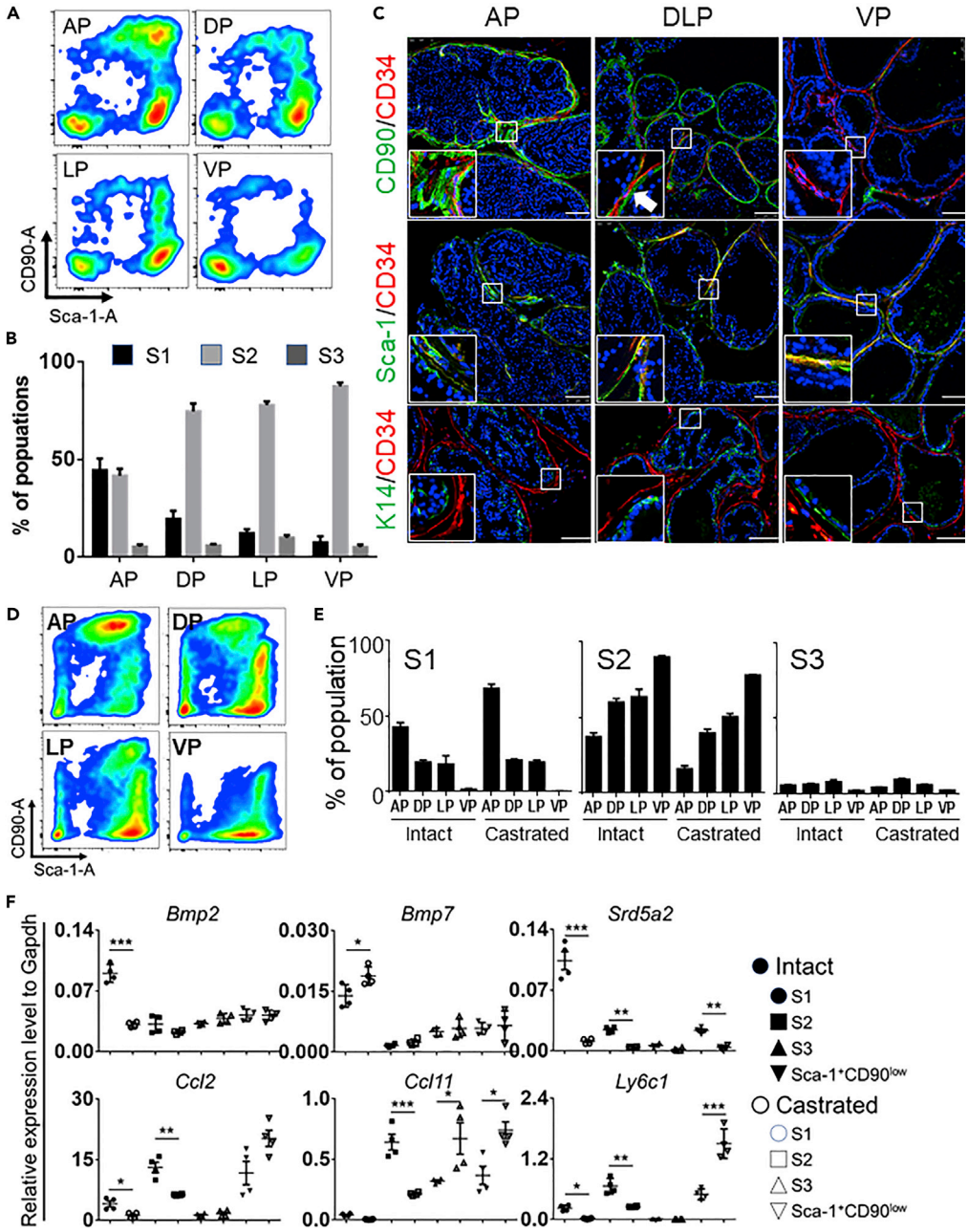

Figure 3. Anatomic Distribution and Hormonal Regulation of Distinct Prostate Stromal Cells

(A) FACS plot shows that each lobe has different percentage of subpopulations. AP: anterior prostate, DP: dorsal prostate, LP: lateral prostate, VP: ventral prostate.

(B) Bar graph shows means ± SEM of percentage of each subpopulation in different lobes from three independent experiments.

(C) Coimmunostaining of CD34/CD90, CD34/Sca-1, and K14/CD34 in different prostate lobes. White arrow denotes that $CD34^+$ stromal cells are located outside of $CD90^+$ stromal cells. Scale bars, 100 μm. DLP: dorsolateral prostate.

(D and E) (D) FACS plot and (E) bar graph show means ± SEM of percentages of individual subpopulations in prostate of castrated mice.

(F) qRT-PCR analysis for representative genes associated with R1 and R2 cells in stromal subpopulations from intact and castrated mice. Dot plots show means ± SEM of relative expression to *Gapdh*. N=4. *$p < 0.05$, **$p < 0.01$, ***$p < 0.001$.

See also Figure S3.

mostly mark different stromal cell populations, which is also consistent with the FACS analysis (Figure S1D). More interestingly, $CD90^+$ stromal cells are in direct contact with the epithelial cells, whereas the $CD34^+$ and $Sca\text{-}1^+$ cells are localized outside the layer of the $CD90^+$ cells (white arrow in the inset in the of middle image of top panel, Figure 3C).

We then investigated how the stromal cell subpopulations change in response to androgen deprivation. Figures 3D and 3E show that the overall pattern of the proportions of individual stromal subpopulations did not alter drastically in the castrated mice, except that the $CD90^-$ and $CD90^{low}$ populations within the $Sca\text{-}1^+CD90^{-/low}$ S2 cells became more distinctive (Figure 3D). qRT-PCR analysis of several representative genes associated with the R1–R2 subpopulations reveals that the $Sca\text{-}1^+CD90^{low}$ cells in castrated mice display a similar gene expression profile with both the $Sca\text{-}1^+CD90^{-/low}$ total S2 cells and the $Sca\text{-}1^+CD90^{low}$ S2 cells in intact mice (Figure 3F), suggesting that these cells are not the S1 cells that had a reduced CD90 expression in response to androgen deprivation. Although androgen deprivation did not alter the phenotypic appearance of individual stromal cell populations, it downregulated *Bmp2* and *Srd5a2* but upregulated *Bmp7* in the S1 cells and downregulated *Ccl2*, *Ccl11*, and *Ly6c1* in the S2 cells (Figure 3F).

Previous study has shown that high fat diet can induce a very mild inflammatory microenvironment in the prostate (Kwon et al., 2016). We therefore investigated how the stromal cell subpopulations were affected by high-fat diet. Figures S3D and S3E shows that there was no drastic change in the phenotypic profile and proportion of individual stromal subpopulations in mice fed with high-fat diet. *Ccl2* was upregulated in the S2 cells in the high-fat-diet-fed group, corroborating a mild prostate inflammation induced by high-fat diet (Figure S3F). However, there was no widespread change in the expression of representative genes associated with individual populations except that *Bmp7* and *Wif1* were downregulated in the S1 cells and *Fn1* was downregulated in the S2 cells.

Distinct Impact of Different Stromal Cell Lineages on Basal Cell Differentiation

Prostate stromal cells have been shown to regulate epithelial cell survival and proliferation via juxtacrine or paracrine signaling (Marker et al., 2003). We employed a previously established prostate organoid assay (Karthaus et al., 2014) to determine whether different stromal cell populations may affect the organoid-forming capability of the prostate basal cells and their differentiating capacity. Briefly, FACS-isolated adult mouse prostate basal ($Lin^-Sca\text{-}1^+CD49f^+$) cells were cultured in the organoid assay alone, or cocultured with FACS-isolated S1 and S2 cells separately. To test whether cross talk between S1 and S2 cells is necessary for them to regulate basal epithelial stem cell activity, we included a fourth group in which basal cells were cocultured with both S1 and S2 cells. Figure 4A shows that the organoid-forming activity of the basal cells is increased by 1.27 to 1.38-fold in all the three coculture groups compared with that in the control group with the basal cells only. FACS-sorted stromal cells do not form organoids when cultured alone (organoid-forming unit <1/4,000, Figure S4A). The stromal cells can survive during the 7- to 10-day culture in the organoid culture condition. They did not undergo senescence as measured by qRT-PCR analysis of the senescence markers *p16* and *p19* (Figure S4B). Neither did they proliferate during the culture (Figure S4C). Therefore the increased organoid-forming unit was from the basal cells. In addition, the size of the organoid was also increased by 1.08 to 1.15-fold significantly (Figure 4B). By coculturing the stromal cells expressing tdTomato with wild-type basal cells, we showed that the stromal cells did not incorporate into the basal-cell-derived organoids (Figure S4D). Therefore the increased organoid size likely reflects an increase in the proliferation of the organoid cells.

The majority (96.7%) of the organoids formed in the control group are composed of cells that express both the basal cell marker cytokeratin 5 (K5) and the luminal cell marker cytokeratin 8 (K8) (hereafter referred to as the Type I organoid, Figure 4C). In contrast, the remaining 3.3% of organoids consists of cells that highly express K5 but with a weak expression of K8 (hereafter referred to as the Type II organoids, Figure 4C). These two types of organoids may reflect either the differentiation status of the organoid cells or different features of their respective cellular origins.

Interestingly, coculture of the basal cells with different types of stromal cells significantly increased the percentage of the Type II organoids (19.5% and 74.1% in the S1 and S2 coculture, respectively) (Figure 4D). The percentage of the Type II organoids in the coculture group with both the S1 and S2 cells (23.8%) fell between those of the S1 coculture and S2 coculture groups, which suggests that there is no synergy or interference between the two stromal cell populations in this assay. As the increase in the organoid-forming

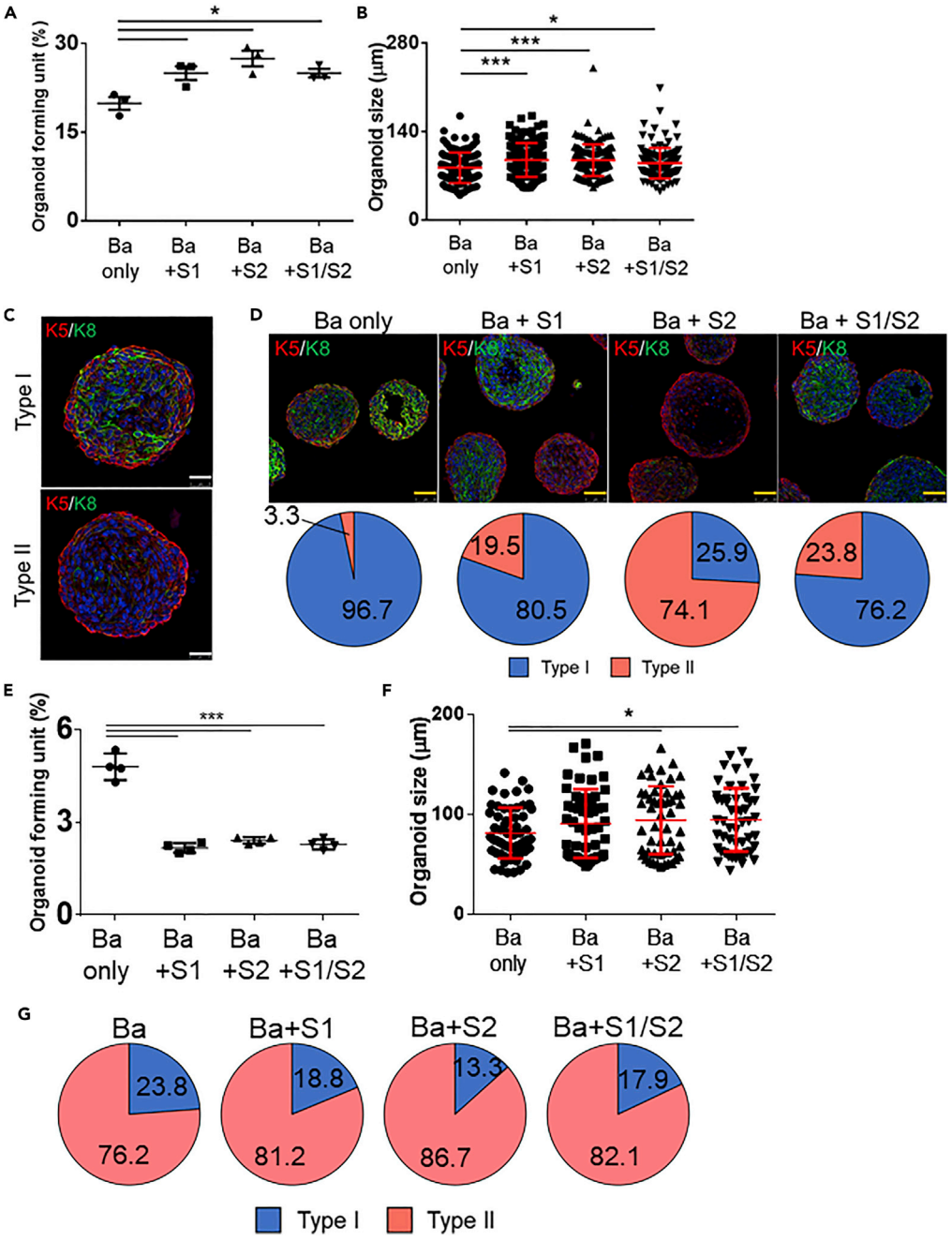

Figure 4. S2 Cells Suppress Bipotent Differentiation of Prostate Basal Cells

(A) Dot plot shows means ± SD of organoid-forming units of basal cell (Ba) when cultured alone or with stromal subpopulation (S1, S2, or the mixture of S1 and S2). Results were from three independent experiments. *$p < 0.05$.

(B) Dot plot shows means ± SD of organoid size. *$p < 0.05$, ***$p < 0.001$.

(C) Coimmunostaining of keratin 5 (K5) and keratin 8 (K8) in Type I and Type II organoids. Scale bars, 25 μm.

(D) Coimmunostaining of K5 and K8 in organoids derived from basal cells when cultured alone or with stromal subpopulations. Pie charts quantify types of organoids. Scale bars, 50 μm.

(E) Dot plot shows means ± SD of organoid-forming units from passaged organoid. ***$p < 0.001$.

(F) Dot plot shows means ± SD of size of passaged organoid. *$p < 0.05$.

(G) Pie charts quantify types of passaged organoids.

See also Figure S4.

activity is minor, we believe that the increased frequency of the type II organoids is not because the S1 and S2 cells can promote the survival and growth of a basal cell subpopulation that specifically generate the Type II organoids. Instead, this observation supports that the S1 and S2 stromal cells suppress bipotent differentiation of the basal cells.

To determine whether such activity is mediated via direct cell-cell contact or paracrine signaling, we suspended FACS-sorted prostate basal cells and stromal cells in Matrigel separately so that they were cocultured in the organoid assay but did not contact directly. We obtained very similar results (Figures S4E and S4F), which supports the fact that the stromal cells suppress bipotent differentiation of the basal cells in the organoid assay in a paracrine manner. Figures S4G and S4H show that even after coculture with the basal cells, the S1 and S2 cells still retained their molecular and phenotypic properties. Together, these results suggest that the distinct capacity of the S1 and S2 cells to suppress bipotent differentiation of basal cells in the organoid assay is determined by their different secretomes.

To determine whether coculture of the basal cells with stromal cells affects their capacity for self-renewal, we FACS-sorted basal cells in each organoid culture shown in Figure 4D and passaged them alone, separately. Figure 4E shows that the organoid-forming activities were all decreased in the secondary culture, but the reduction was more significant in the coculture groups (from 19.9% to 4.8% in the basal cell alone group versus from 25.8% to 2.3% in the coculture groups). The sizes of the organoids in the S2 and S1 + S2 group were slightly bigger than that in the control group (1.15- to 1.17-fold) (Figure 4F). Surprisingly, in all the cultures, the Type II organoid became the predominant type of the organoids (Figure 4G). This implies that during the organoid culture the FACS-sorted basal cells have changed. They lost some bipotent differentiation capacity and became committed to unipotent basal cells. Coculturing with the stromal cells accelerates this process in the organoid assay.

DISCUSSION

Distinct Stromal Cell Populations with Possibly Specialized Functions

We separated prostate stromal cells into three major populations (R1–R3) with distinct biological functions using scRNA-seq. Based on the information obtained from the scRNA-seq we were able to identify surface antigens that distinguish two of the three populations: the Sca-1^{+}CD90^{+} (S1) and Sca-1^{+}CD90$^{-/low}$ (S2) stromal cells roughly correspond to the R1 and R2 cells, respectively. Both cell populations display a fibroblastic phenotype based on their expression of representative fibroblast cell-associated genes, but the R1 cells express the fibroblastic cell marker *Vimentin* at a relatively lower level compared with the R2 cells. The R2 cells highly express *S100a4* and *Acta2* as well as many inflammation-associated genes, suggesting a myofibroblast phenotype. It should be noted that Sca-1 and CD90 only separate stromal cells into rough subpopulations and that other markers are necessary to further define purer stromal subpopulations in the mouse prostate.

The R1 cells express various growth factors, including *Bmp*s and *Wnt*s, as well as *Srd5a2*, the essential enzyme for DHT synthesis. These features suggest that the CD90^{+} cells play an important role in the growth and androgen-mediated survival of prostate epithelial cells. This is further supported by the fact that these cells are in direct contact with the epithelial cells. The features of these cells are similar to those of the telocytes reported in the small intestines (Shoshkes-Carmel et al., 2018), suggesting that they may share the same developmental origin or differentiation trajectories. The growth factors and DHT generated by these cells are easily accessible to the epithelial cells via paracrine signaling. DHT may also be transported to epithelial cells via gap junctions. Interestingly, *Srd5a2*, an enzyme critical for DHT synthesis, is downregulated in the S1 cells after castration. These observations indicate that the CD90^{+} stromal cells may play a critical role in the androgen-regulated survival of prostate epithelial cells. It is interesting that the CD90^{+} cells are rare in the ventral prostate lobes that are more resistant to androgen deprivation than the other prostate lobes (O.-J.K. and X.W., unpublished data). This suggests that the epithelial cells in ventral prostate lobes may employ distinct signaling to maintain their growth and survival after androgen ablation.

R3 cells consist of cells that are phenotypically smooth muscle cells. Genes involved in tissue development and homeostasis, neurogenesis, and angiogenesis are also highly expressed by these cells, suggesting that the smooth muscle cells carry other important functions than the simple supporting and contractile roles. Unfortunately, we were not able to identify a combination of surface markers that can specifically separate the R3 cells. It is possible that the smooth muscle cells are more susceptible to the mechanical and enzymatic digestion during single-cell preparation, and thereby are partially depleted during the assay

(the S4 cell debris in Figure 2A). In addition, CD90 and Sca-1 are not enough to distinguish the R3 cells from the other cell populations as our qRT-PCR analysis showed that the genes highly expressed in the R3 cells (Figure 1C) can be detected in both the S2 and S3 cells. Other markers are necessary to isolate this cell population in the future.

Fibroblast and myofibroblast have been shown to undergo phenotypic conversion between each other upon stimulation such as mechanical tension (Meran and Steadman, 2011). Interestingly, we showed that even after extended *in vitro* culture, the phenotypic profiles of S1 and S2 cells, such as the expression of surface antigens and specific genes, are relatively stable. This observation indicates that they may have distinct developmental origins that shape their molecular phenotypes and functional properties. This is also consistent with the previous study showing that different types of stromal cells in the mouse prostate are independently sustained (Peng et al., 2013). Future studies using lineage tracing should be able to corroborate this theory more definitively.

Stromal Regulation of Basal Cell Differentiation

The prostate organoid assay provides a permissive environment for the prostate basal cells to survive, proliferate, and undergo differentiation to generate cells with a luminal phenotype. We showed that coculture of the basal cells with the S1 and especially S2 cells block the luminal differentiation of the basal cells. Basal-to-luminal differentiation is often associated with an increase in cellular proliferation (Karthaus et al., 2014; Lamb et al., 2010; Xin et al., 2003). For example, when basal cells are cultured in Petri dish stimulated with growth factors they can proliferate and differentiate. In addition, we showed previously that prostate inflammation can induce basal-to-luminal differentiation, which is also accompanied by increased cellular proliferation. Therefore, it is surprising that the cytokine-producing Sca-1^{+}CD90$^{-/low}$ cells can stimulate organoid growth yet suppress differentiation. This indicates that the inflammatory and growth-stimulating signaling *in vivo* and in the organoid assay are not completely the same. Alternatively, direct interaction of basal cells with immune cells may play a role in basal-to-luminal differentiation.

One suspected candidate signaling through which S1 and S2 cells block basal-to-luminal differentiation is the Wnt signaling because it has been reported to be necessary for basal-to-luminal differentiation (Lu and Chen, 2015; Madueke et al., 2018). The Wnt agonist R-spondin is an essential component for organoid growth (Karthaus et al., 2014; Kwon et al., 2015). Nevertheless, removing R-spondin or adding the Wnt inhibitor IWP-2 in the organoid assay only reduces the number and size of the organoids, but not the differentiation status of the cells (Figures S4I and S4L). In addition, the S2 cells do not always express the various Wnt inhibitors more than the S1 cells (Figure S4M). Therefore it is unlikely that the S2 cells block basal-to-luminal differentiation by interfering with the Wnt signaling in the basal cells in the organoid assay. Future gene expression and proteomic profiling may provide more insights into the underlying mechanisms.

Limitations of the Study

We classify the mouse prostate stromal cells into three distinct populations in this study. These populations are also heterogeneous and should be able to be further subclassified by additional studies including more cells with deeper reads.

METHODS

All methods can be found in the accompanying Transparent Methods supplemental file.

DATA AND SOFTWARE AVAILABILITY

The accession numbers for the single cell RNA-seq data is GEO: GSE119988.

SUPPLEMENTAL INFORMATION

Supplemental Information can be found online at https://doi.org/10.1016/j.isci.2019.02.032.

ACKNOWLEDGMENTS

We thank the technical support by the Cytometry and Cell Sorting Core at Baylor College of Medicine with funding from the NIH (P30 AI036211, P30 CA125123, and S10 RR024574) and the expert assistance of Joel M. Sederstrom. This work is supported by NIH R01 DK092202 and DK107436 (L.X.).

AUTHOR CONTRIBUTIONS

O.-J.K. and L.X. designed the experiments. O.-J.K., Y.L., X.W., and L.Z. performed experiments, acquired the data, and analyzed the data. Y.Z. and C.J.C. analyzed the data. L.X. wrote the manuscript with input from C.J.C. and O.-J.K.

DECLARATION OF INTERESTS

The authors declare no competing interests.

Received: September 19, 2018
Revised: January 23, 2019
Accepted: February 27, 2019
Published: March 29, 2019

REFERENCES

Barron, D.A., and Rowley, D.R. (2012). The reactive stroma microenvironment and prostate cancer progression. Endocr. Relat. Cancer *19*, R187–R204.

Brennen, W.N., Denmeade, S.R., and Isaacs, J.T. (2013). Mesenchymal stem cells as a vector for the inflammatory prostate microenvironment. Endocr. Relat. Cancer *20*, R269–R290.

Brennen, W.N., Kisteman, L.N., and Isaacs, J.T. (2016). Rapid selection of mesenchymal stem and progenitor cells in primary prostate stromal cultures. Prostate *76*, 552–564.

Cunha, G.R., and Ricke, W.A. (2011). A historical perspective on the role of stroma in the pathogenesis of benign prostatic hyperplasia. Differentiation *82*, 168–172.

Kalluri, R. (2016). The biology and function of fibroblasts in cancer. Nat. Rev. Cancer *16*, 582–598.

Karthaus, W.R., Iaquinta, P.J., Drost, J., Gracanin, A., van Boxtel, R., Wongvipat, J., Dowling, C.M., Gao, D., Begthel, H., Sachs, N., et al. (2014). Identification of multipotent luminal progenitor cells in human prostate organoid cultures. Cell *159*, 163–175.

Kim, W., Barron, D.A., San Martin, R., Chan, K.S., Tran, L.L., Yang, F., Ressler, S.J., and Rowley, D.R. (2014). RUNX1 is essential for mesenchymal stem cell proliferation and myofibroblast differentiation. Proc. Natl. Acad. Sci. U S A *111*, 16389–16394.

Kwon, O.J., Zhang, B., Zhang, L., and Xin, L. (2016). High fat diet promotes prostatic basal-to-luminal differentiation and accelerates initiation of prostate epithelial hyperplasia originated from basal cells. Stem Cell Res. *16*, 682–691.

Kwon, O.J., Zhang, L., and Xin, L. (2015). Stem cell antigen-1 identifies a distinct androgen-independent murine prostatic luminal cell lineage with bipotent potential. Stem Cells *34*, 191–202.

Lamb, L.E., Knudsen, B.S., and Miranti, C.K. (2010). E-cadherin-mediated survival of androgen-receptor-expressing secretory prostate epithelial cells derived from a stratified in vitro differentiation model. J. Cell Sci. *123*, 266–276.

Lawson, D.A., and Witte, O.N. (2007). Stem cells in prostate cancer initiation and progression. J. Clin. Invest. *117*, 2044–2050.

Lin, V.K., Wang, S.Y., Vazquez, D.V., C Xu, C., Zhang, S., and Tang, L. (2007). Prostatic stromal cells derived from benign prostatic hyperplasia specimens possess stem cell like property. Prostate *67*, 1265–1276.

Lu, T.L., and Chen, C.M. (2015). Differential requirements for beta-catenin in murine prostate cancer originating from basal versus luminal cells. J. Pathol. *236*, 290–301.

Madueke, I.C., Hu, W.Y., Huang, L., and Prins, G.S. (2018). WNT2 is necessary for normal prostate gland cyto-differentiation and modulates prostate growth in an FGF10 dependent manner. Am. J. Clin. Exp. Urol. *6*, 154–163.

Marker, P.C., Donjacour, A.A., Dahiya, R., and Cunha, G.R. (2003). Hormonal, cellular, and molecular control of prostatic development. Dev. Biol. *253*, 165–174.

Meran, S., and Steadman, R. (2011). Fibroblasts and myofibroblasts in renal fibrosis. Int. J. Exp. Pathol. *92*, 158–167.

Ohlund, D., Elyada, E., and Tuveson, D. (2014). Fibroblast heterogeneity in the cancer wound. J. Exp. Med. *211*, 1503–1523.

Papalexi, E., and Satija, R. (2017). Single-cell RNA sequencing to explore immune cell heterogeneity. Nat. Rev. Immunol. *18*, 35–45.

Peng, Y.C., Levine, C.M., Zahid, S., Wilson, E.L., and Joyner, A.L. (2013). Sonic hedgehog signals to multiple prostate stromal stem cells that replenish distinct stromal subtypes during regeneration. Proc. Natl. Acad. Sci. U S A *110*, 20611–20616.

Risbridger, G.P., and Taylor, R.A. (2008). Minireview: regulation of prostatic stem cells by stromal niche in health and disease. Endocrinology *149*, 4303–4306.

Shibata, M., and Shen, M.M. (2013). The roots of cancer: stem cells and the basis for tumor heterogeneity. BioEssays *35*, 253–260.

Shoshkes-Carmel, M., Wang, Y.J., Wangensteen, K.J., Toth, B., Kondo, A., Massassa, E.E., Itzkovitz, S., and Kaestner, K.H. (2018). Subepithelial telocytes are an important source of Wnts that supports intestinal crypts. Nature *557*, 242–246.

Strand, D.W., Costa, D.N., Francis, F., Ricke, W.A., and Roehrborn, C.G. (2017). Targeting phenotypic heterogeneity in benign prostatic hyperplasia. Differentiation *96*, 49–61.

Sun, Y.B., Qu, X., Caruana, G., and Li, J. (2016). The origin of renal fibroblasts/myofibroblasts and the signals that trigger fibrosis. Differentiation *92*, 102–107.

Treutlein, B., Brownfield, D.G., Wu, A.R., Neff, N.F., Mantalas, G.L., Espinoza, F.H., Desai, T.J., Krasnow, M.A., and Quake, S.R. (2014). Reconstructing lineage hierarchies of the distal lung epithelium using single-cell RNA-seq. Nature *509*, 371–375.

Wang, Z., Hu, L., Salari, K., Bechis, S.K., Ge, R., Wu, S., Rassoulian, C., Pham, J., Wu, C.L., Tabatabaei, S., et al. (2017). Androgenic to oestrogenic switch in the human adult prostate gland is regulated by epigenetic silencing of steroid 5alpha-reductase 2. J. Pathol. *243*, 457–467.

Wollny, D., Zhao, S., Everlien, I., Lun, X., Brunken, J., Brune, D., Ziebell, F., Tabansky, I., Weichert, W., Marciniak-Czochra, A., et al. (2016). Single-cell analysis uncovers clonal acinar cell heterogeneity in the adult pancreas. Dev. Cell *39*, 289–301.

Xin, L. (2013). Cells of origin for cancer: an updated view from prostate cancer. Oncogene *32*, 3655–3663.

Xin, L., Ide, H., Kim, Y., Dubey, P., and Witte, O.N. (2003). In vivo regeneration of murine prostate from dissociated cell populations of postnatal epithelia and urogenital sinus mesenchyme. Proc. Natl. Acad. Sci. U S A *100* (*Suppl 1*), 11896–11903.

Xin, L., Lawson, D.A., and Witte, O.N. (2005). The Sca-1 cell surface marker enriches for a prostate-regenerating cell subpopulation that can initiate prostate tumorigenesis. Proc. Natl. Acad. Sci. U S A *102*, 6942–6947.

ISCI, Volume *13*

Supplemental Information

Functional Heterogeneity of Mouse Prostate Stromal Cells Revealed by Single-Cell RNA-Seq

Oh-Joon Kwon, Yiqun Zhang, Yumei Li, Xing Wei, Li Zhang, Rui Chen, Chad J. Creighton, and Li Xin

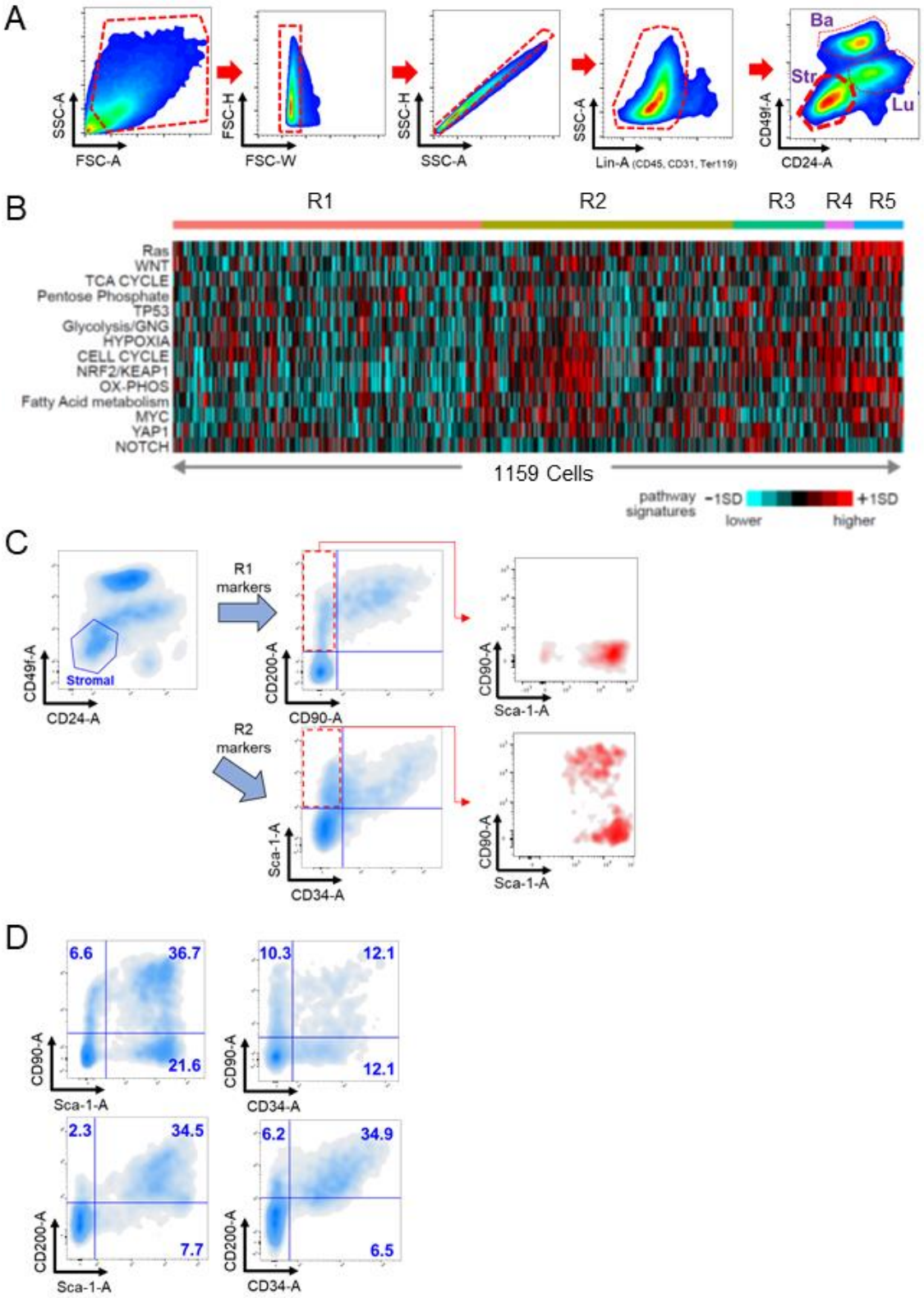

Supplementary Figure 1: Separating prostate stromal cells by surface markers. Related to Figure 1.

A: FACS plots of prostate cell lineages in 10-week-old wild type mice using lineage markers (CD45, CD31, and Ter119), CD49f, and CD24. B: Pathway-associated mRNA signatures of prostate stromal cell subpopulations. Gene transcription signature scores associated with specific pathways (e.g. scores for p53, NRF2/KEAP1, hypoxia, KEGG: Glycolysis/Gluconeogenesis, KEGG: Pentose Phosphate pathway, KEGG: Fatty Acid metabolism, KEGG: TCA Cycle, and KEGG: Oxidative Phosphorylation or OX-PHOS, k-ras, MYC, YAP1, WNT, and NOTCH) were computed with pathway scores normalized to standard deviations from average across cells. Gene features detected in more than 10 cells were utilized in this analysis. C: FACS plots of stromal cells using R1 cell-enriched markers (CD90 and CD200) and R2 cell-enriched markers (Sca-1 and CD34). D: FACS plots of stromal cells with different combinations of surface markers.

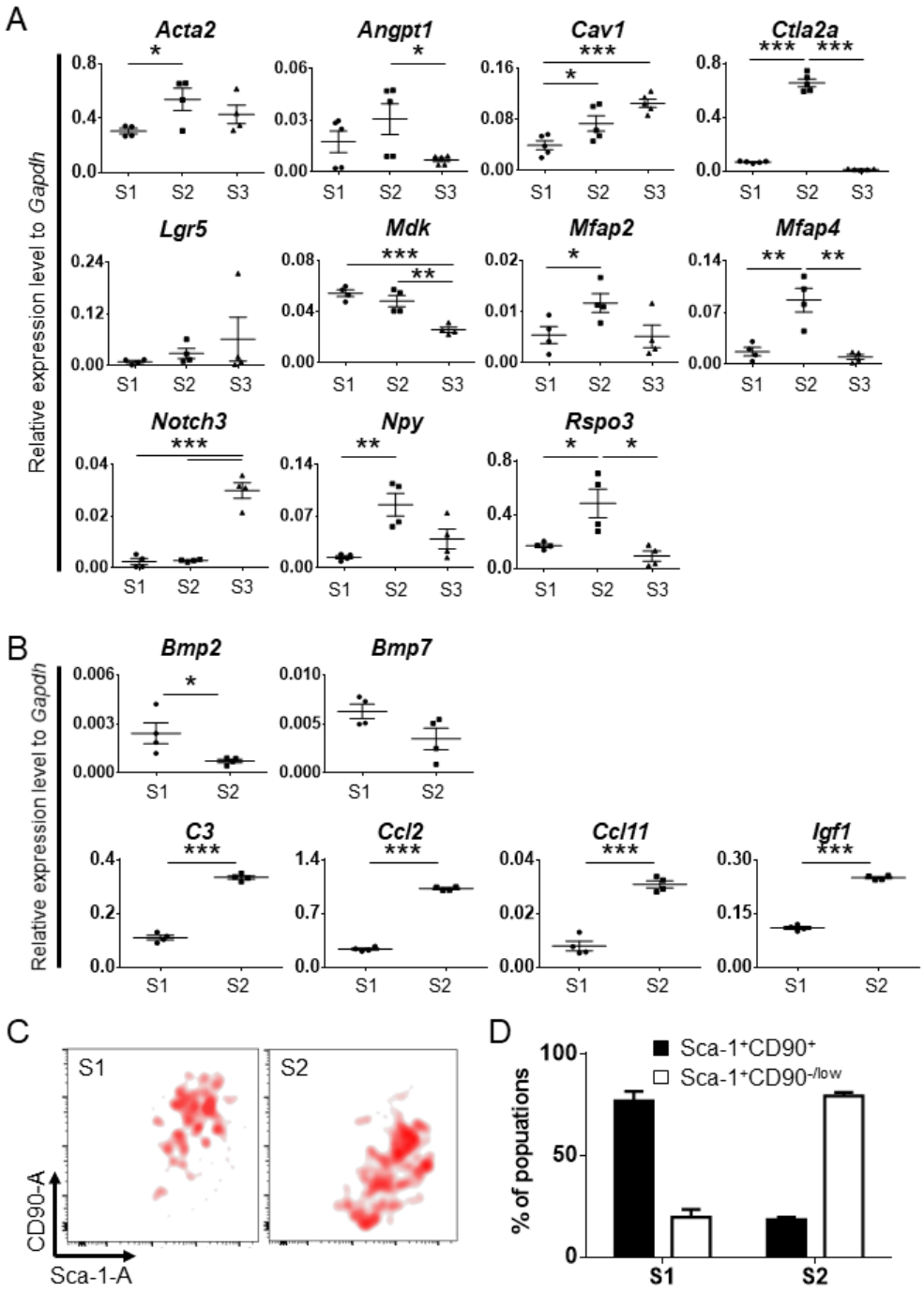

Supplementary Figure 2. Sca-1 and CD90 fractionates prostate stromal cells. Related to Figure 2. A: QRT-PCR analysis of R3 cell-related genes in FACS-sorted prostate stromal subpopulations. Results show means ± SD of relative expression level to *Gapdh* from four independent experiments. *: p<0.05. **: p<0.01. ***: p<0.001. B: qRT-PCR analysis of representative genes of R1 and R2 in S1 and S2 stromal cells that have been cultured in vitro in petridish for 7 days. Results show means ± SD of relative expression to *Gapdh* from 4 independent experiments. *: p<0.05. ***: p<0.001. C-D: Representative FACS plots of Sca-1 and CD90 in S1 and S2 stromal cells that have been cultured in vitro in petridish. Bar graph shows means ± SD of percentage of cells from 3 independent experiments.

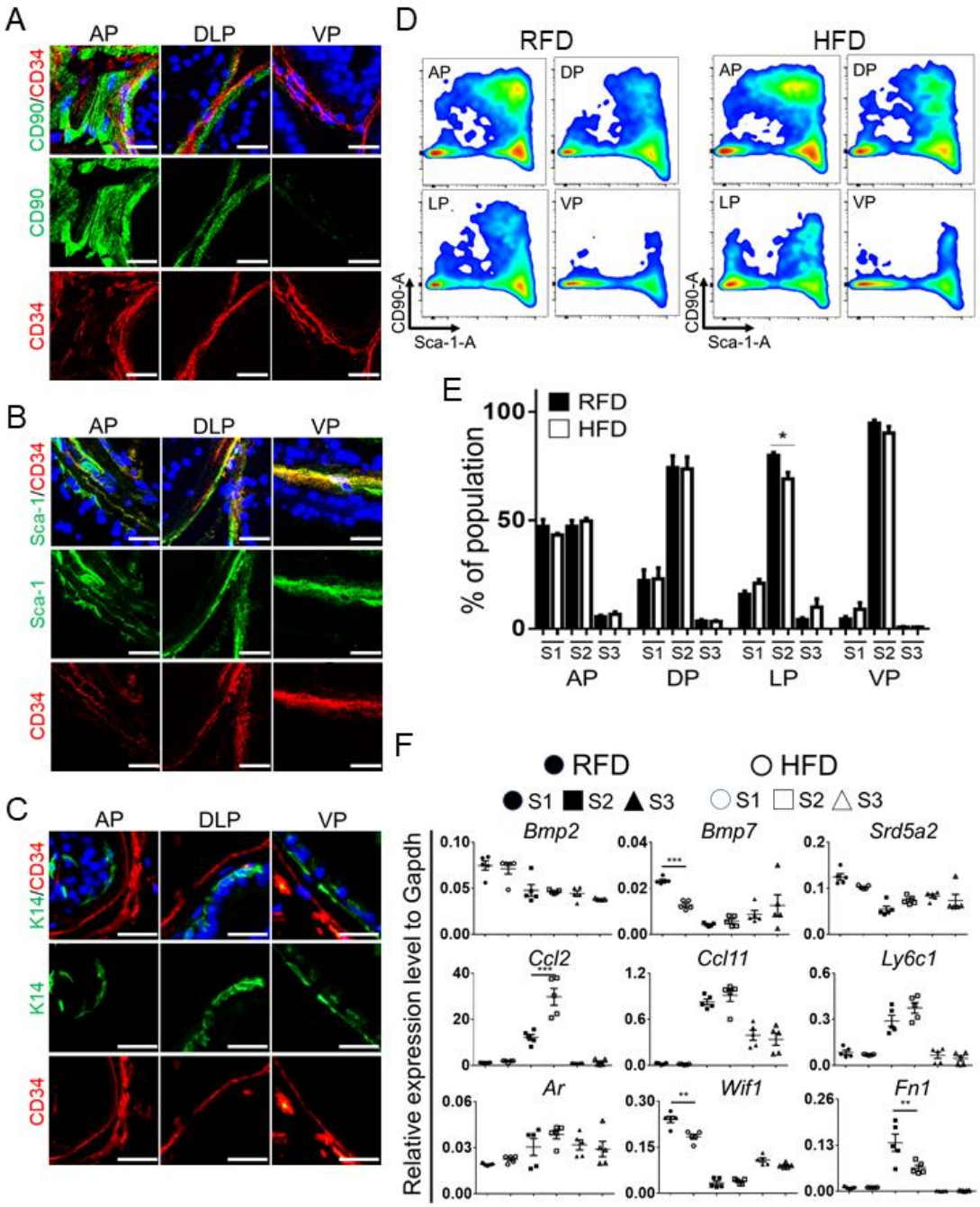

Supplementary Figure 3. Anatomic distribution and hormonal regulation of distinct prostates stromal cells. Related to Figure 3.

A-C: Coimmunostaining of CD34/CD90 (A), CD34/Sca-1 (B), and CD34/K14 (C) in different prostate lobes. Bars=25 μm. D: FACS plots show stromal subpopulations in individual prostatic lobes of mice fed with regular fat diet (RFD) and high fat diet (HFD), respectively. E: Bar graph shows means ± SEM of percentage of each subpopulation in different lobes from 3 independent experiments. *: $p<0.05$. F: qRT-PCR analysis of representative genes associated with R1 and R2 cells in FACS-isolated S1, S2 and S3 cells in RFD and HFD groups. Result shows means ± SD of relative expression level to *Gapdh* from 5 independent experiments. *: $p<0.05$. **: $p<0.01$. ***: $p<0.001$.

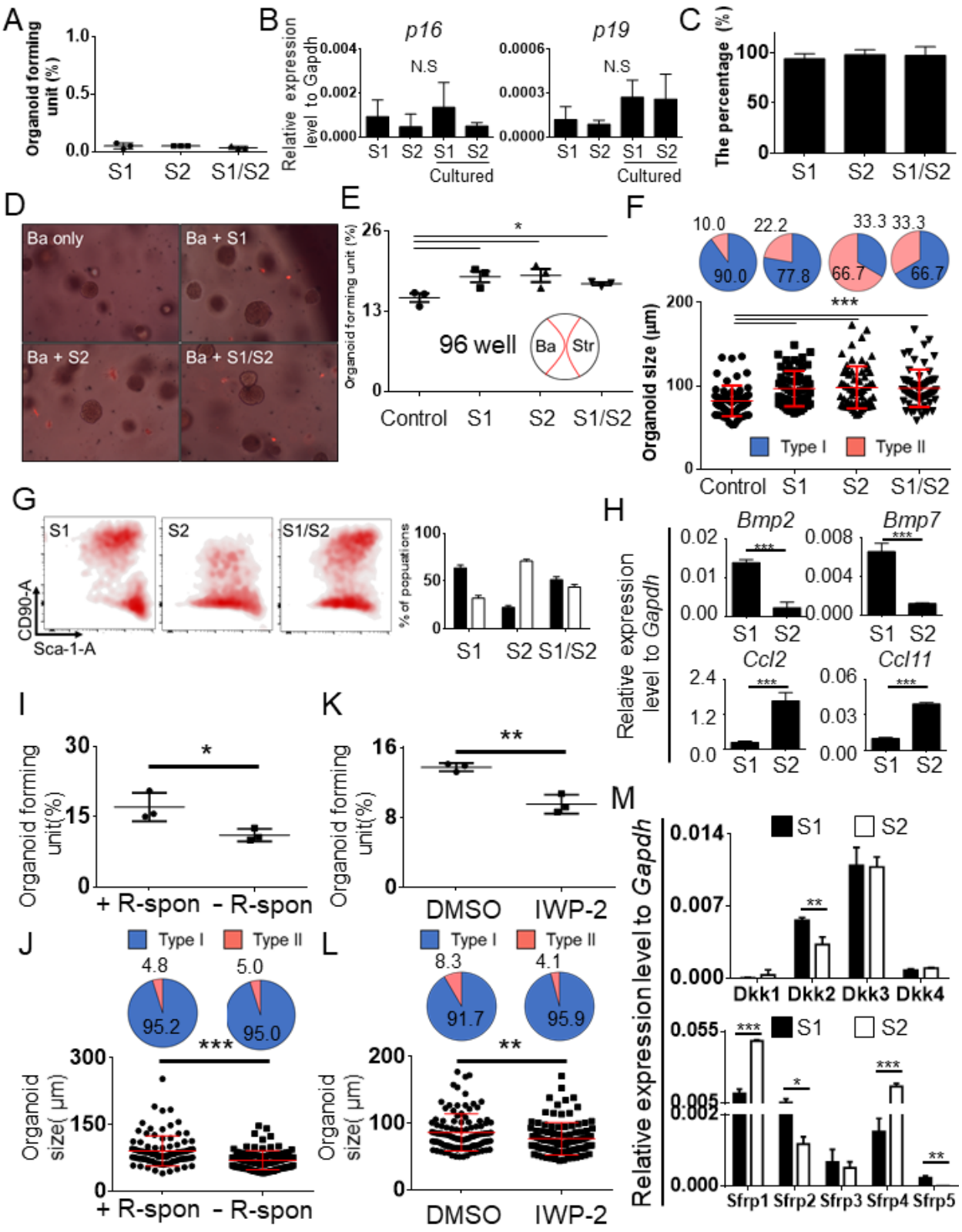

Supplementary Figure 4. S2 cells suppress bipotent differentiation of prostate basal cells. Related to Figure 4.

A: Dot plot shows means ± SD of organoid-forming unit from FACS-isolated stromal subpopulations. B: qRT-PCR analysis shows means ± SD of relative expression level of senescence markers, *p16* and *p19*, to *Gapdh* in freshly FACS sorted stromal cells and *in vitro* cultured stromal cells. n.s.: not significant. C: Bar graph shows means ± SD of percentage of viable stromal cells after in vitro culture in organoid culture media for 7 days. D: Overlaid images of transillumination and fluorescence show coculture of FACS-isolated basal cells from C57Bl/6 mice and stromal cells from mTmG mice in organoid assay. Ba: basal cells. S1: Lin^- $Sca\text{-}1^+CD90^+$ cells. S2: $Lin^-Sca\text{-}1^+CD90^{-/low}$ cells. E: Dot plot shows means ± SD of organoid forming units of FACS-isolated basal cells when cultured alone or with S1, S2, and S1+S2 cells separately but without direct contact. Inset image shows that basal cells and stromal cells were immobilized separately in Matrigel at opposite side of a well in 96-well plate. Results were from 3 independent experiments. *: $p<0.05$. F: Dot plot shows means ± SD of organoid size and pie charts quantify the types of organoids. ***: $p<0.001$. G: FACS plots show staining of Sca-1 and CD90 in stromal cells after coculture in organoid assay with basal cells. Bar graph shows means ± SD of cellular percentage. H: qRT-PCR analysis of *Bmp2*, *Bmp7*, *Ccl2*, and *Ccl11* in stromal cells that have been cocultured with basal cells in organoid assay. Bar graph shows means ± SD of relative expression level to *Gapdh*. I: Dot plot shows means ± SD of organoid-forming units with or without R-spondin in organoid culture media from 3 independent experiments. *: $p<0.05$. J: Dot plot shows means ± SD of organoid size and pie charts quantify the types of organoids. ***: $p<0.001$. K: Dot plot shows ± SD of organoid-forming unit with DMSO or IWP-2 in organoid culture media from 3 independent experiments. **$p<0.01$. L: Dot plot shows means ± SD of organoid size and pie charts quantify the types of organoids. **: $p<0.01$. M: qRT-PCR analysis of expression of endogenous Wnt inhibitors in S1 and S2 cells. Bar graph shows means ± SD of relative expression level to *Gapdh*. *: $p<0.05$. **: $p<0.01$. ***: $p<0.001$.

Supplementary Table 1: Antibodies for Flow cytometry. Related to Figs. 2, 3, and 4.

Antigen	Supplier and catalogue number	Dilution
CD45	eBioscience, 48-0459-41	1:200
CD31	eBioscience, 48-0311-80	1:200
Ter119	eBioscience 48-5921-82	1:200
CD49f	BioLegend, 313616	1:100
CD49f	BioLegend, 313621	1:100
CD24	BD Biosciences, 553261	1:50
Sca-1	eBioscience, 25-5981-81	1:200
Sca-1	eBioscience ,12-5981-83	1:200
CD90.2	eBioscience, 46-0903-80	1:100
CD90.2	BeioLegend, 105307	1:100
CD90.2	eBioscience, 47-0902-82	1:100
CD34	BioLegend, 119307	1:100
CD200	BioLegend, 123810	1:100
BrdU	eBioscience, 11-5071-42	1:200

Supplementary Table 2. Primers for qRT-PCR analysis. Related to Figs 2 and 3.

Gene	Forward	Reverse
Acta2	AGATCAAGATCATTGCCCC	TTCATCGTATTCCTGTTTGC
Angpt1	CAGCATCTGGAGCATGTGAT	GTTGTATCTGGGCCATCTCC
Ar	AATGAGTACCGCATGCACAA	CCCATCCACTGGAATAATGC
Bmp2	GCAGCTTCCATCACGAAGA	CGTCACTGGGGACAGAACTT
Bmp7	ACTACATCCGGGAGCGATTT	GCTGTCCAGCAAGAAGAGGT
C3	GAGCGAAGAGACCATCGTACT	TCTTTAGGAAGTCTTGCACAGTG
Cav1	GCACACCAAGGAGATTGACC	TCCCTTCTGGTTCTGCAATC
Ccl2	AAGAAGATCACCAGCAGCAG	TCTGGACCCATTCCTTCTTG
Ccl11	ATGCACCCTGAAAGCCATAG	CTTCTTCTTGGGGTCAGCAC
CD34	GGACAGCAGTAAGACCACACC	TGGAGTTCCAGAGCCTGAAG
Ctla2a	ACATGGGCCTGAATCAATTT	GCAAATCAGGAGCCATTTCT
Dkk1	GGCTCTGCTGTCAGTGTGG	CATCTTCAGCGCAAGGGTAG
Dkk2	TCAGTCAGCCAACCGATCTG	TCTCTGTGGCATCGTTTCTTTT
Dkk3	ACCAGAGTGGACAGGTGGTC	GGCCCACAGTCTTCATCAAT
Dkk4	CGTAGAGTTCGCAGGAGGTG	ACTGGCCTTGTGTCTTCCAC
Esr1	TGATGATTGGTCTCGTCTGG	CCATGCCTTCCACACATTTA
Esr2	AAGAGTCCTTGGTGTGAAGCA	AGTAACAGGGCTGGCACAAC
Ddr2	CTATGGCACCCACCACCTAT	GCCAGCAGGATGAAGATGAT
Fn1	TCTGGGACTGTACCTGCATC	TGTAGGACTGACCCCCTTCA
Gapdh	TGTTCCTACCCCCAATGTGT	GGTCCTCAGTGTAGCCCAAG
Gr	CTGACTTCCTTGGGGGCTAT	CTGGACGGAGGAGAACTCAC
Igf1	TGGATGCTCTTCAGTTCGTG	CACAATGCCTGTCTGAGGTG

Lgr5	CAACCTCAGCGTCTTCACCT	AAGCAGAGGCGATGTAGGAG
Ly6a	CCATCAATTACCTGCCCCTA	GGCAGATGGGTAAGCAAAGA
Ly6c1	GCCTCTGATGGATTCTGCAT	AGGGCAGAAAGAAAGGCACT
Mdk	TTGGAGCCGACTGCAAATAC	ATTGTACCGCGCCTTCTTC
Mfap2	GAAGTCATCCCAGCCCCTAC	GTACTGTTCTTCGCGGCAGT
Mfap4	CTGATGCTGATGCTGCTCTC	GGGTTGCTGAAGACAGGACT
Mmp2	CGCTTTTCTCGAATCCATGA	GTCCATCCTTGCCATCAAAT
Notch3	CACGTGTCTTGACCGAATTG	GCAGACACCACCATTGACAC
Npy	AGAGATCCAGCCCTGAGACA	TCACCACATGGAAGGGTCTT
P16	CCGCTGCAGACAGACTGG	CCATCATCATCACCTGAATCG
P19	AAGAGAGGGTTTTCTTGGTG	CATCATCATCACCTGGTCC
Pr	CTATGGCGTGCTTACCTGTG	TGCAGTCATTTCTTCCAGCA
Rspo3	ACACCTTGGAAAGTGCCTTG	ACTCCATTCACTGGCCTCAC
Runx2	AGTAGGTGTCCCGCCTCAG	CCTGCCTGGGATCTGTAATC
Sfrp1	TACCACGGAAGCCTCTAAGC	TGTTCAATGATGGCCTCTGA
Sfrp2	GCTAGTAGCGACCACCTCCT	TTCCATGATGTCGTTGTCGT
Sfrp3	ATGGGCTATGAAGACGAGGA	TCTTACCAAGCCGATCCTTC
Sfrp4	CCGTGGAGTTTGTATCTCTCC	GGACCTTTCTTGCACCATCA
Sfrp5	TGGACAACGACCTCTGCAT	TGTGCTCCATCTCACACTGG
Srd5a2	AAGCCCGGAGAGGTCATCTA	AAGCGTAGCCCATCCATTC
Tcf4	AGGCTATCCTTCCTCCAAGC	AAGGGTCGCTGCTGTGAT
Vim	GGAAACTAATCTGGATTCACTC	CATCTCTAGTTTCAACCGTC
Wif1	GAGTGTCCGGATGGGTTCTTA	GAAGCCAGGAGTGACACACA

TRANSPARENT METHODS

CONTACT FOR REAGENT AND RESOURCE SHARING

Further information and requests for resources and reagents should be directed to and will be fulfilled by the Lead Contact, Li Xin (xin18@uw.edu)

EXPERIMENTAL MODEL

Mice

All animals used in this study received humane care in compliance with the principles stated in the Guide for the Care and Use of Laboratory Animals, NIH Publication, 1996 edition, and the protocol was approved by the Institutional Animal Care Committee of Baylor College of Medicine and the University of Washington. The C57BL/6, C57Bl/6 DIO (diet-induced obese) and DIO control, and Gt(ROSA)26Sor$^{tm4(ACTB-tdTomato,-EGFP)Luo}$ mice were purchased from Jackson Laboratory (Bar Harbor, ME).

Method DETAILS

BrdU treatment and castration

To determine the proliferative index of prostate stromal cells, experimental mice received 80 mg/ kg of BrdU (Sigma, St. Louis, MO) for 5 days via I.P injection before euthanized. For androgen deprivation, experimental mice were castrated at the age of 10 weeks using standard techniques as described previously (Kwon et al., 2016)

Preparation of dissociated single prostate cells

Dissociated prostate cells were prepared as described previously (Valdez et al., 2012). Briefly, mouse prostate tissues were digested in DMEM/F12/Collagenase/Hyaluronidase/FBS (StemCell technologies, Vancouver, Canada) for 3 hours at 37°C, followed by an additional digestion in 0.25% Trypsin-EDTA (Invitrogen, Carlsbad, CA) on ice for 1 hour. Subsequently, digested cells were suspended in Dispase (Invitrogen, Carlsbad, CA, 5 mg/mL) and DNase I (Roche Applied Science, Indianapolis, IN, 1 mg/mL), and pipetted vigorously to dissociate cell clumps. Dissociated cells were then passed through 70 μm cell strainers (BD Biosciences, San Jose, CA) to get single cells.

Flow cytometry and cell sorting

Dissociated single mouse prostate cells were incubated with florescence conjugated antibodies at 4^{o}C for 30 minutes. Information for antibodies for FACS analysis and sorting is listed in Supplementary Table 1. FACS analyses and sorting were performed by using the BD LSR II, and Aria II (BD Biosciences, San Jose, CA) and gating was confirmed using fluorescence minus one.

RNA isolation and quantitative RT–PCR

Total RNA was extracted using Nucleospin RNA XS Kit (Macherey-Nagel, Bethlehem, PA). RNA was reverse transcribed to cDNA using qScript™ cDNA SuperMix (Quanta, Gaithersburg, MD). QRT-PCR was performed using SYBR Green system (Quanta, Gaithersburg, MD) and detected on a StepOne plus Real-Time PCR system (Applied Biosystems, Foster City, CA). Primers for target genes were listed in Supplementary Table 2.

Single cell RNA-seq

FACS-isolated single adult mouse prostate stromal cells were stained with Hoechst 33342 and Propidium iodide (ReadyProbe Cell Viability Imaging kit R37610, Thermo Fisher) to determine concentration of viable cells. Cells were dispensed into printed chip (Takara Bio USA, Mountain View, CA) using MultiSample NanoDispenser (MSND). The chip loaded with cells was imaged using an Olympus BX43 fluorescent microscope to locate wells with single cells using CellSelect software (Takara Bio USA, Mountain View, CA). To break cells for downstream analysis, the chip was frozen at -80°C for more than one hour before thawed. In-chip RT-PCR amplification and the single cell RNA-seq library construction were performed following the iCELL8 single cell polyA transcriptome amplification hands-on workflow checklist and preparation guide. Briefly, RT-PCR reagents (Takara Bio USA, Mountain View, CA, 639537 and 639504) were dispensed into selected wells using MSND and the reaction was carried out on a BioRad T100 thermocycler with a modified plate. cDNA was collected and pooled together. Concentration was measured using the DNA Clean and Concentrator-5 (Zymo Research, Irvine, CA). CDNA was purified using Ampure XP magnetic beads (Beckman Coulter, Brea, CA). 3’ transcriptome enriched library was made using a 3’-specific P5 primer (Takara Bio USA, Mountain View, CA) and a Nextera XT Kit (Illumina, San Diego, CA). Sequencing was

performed on Illumina Hiseq2500 and a total of 146M reads were generated. Sample demultiplexing was performed with custom script to generate sequence file for individual cells.

We processed 1417 individual fastq files (including 48 negative and 46 positive controls) using "top hat" and "cufflinks" in Galaxy (https://usegalaxy.org/). After filtering for cell expression profiles with a minimum of 500 detected genes and alignment rates >40%, 1159 profiles were used in the final analysis. Cell expression profiles were quantile normalized and analyzed using the Seurat R package (http://satijalab.org/seurat/). Using default parameters, Seurat analysis defined cellular subsets. Briefly, Seurat methods embeds cells in a graph structure, with edges drawn between cells with similar gene expression patterns, and then attempts to partition this graph into highly interconnected 'quasi-cliques' or 'communities'. tSNE plots, as generated using Seurat, were used to visualize the cellular subsets, although the clustering approach of Seurat involves methods that are independent of the tSNE components. For each Seurat subgroup, we defined the top associated over-expressed genes, by p-value using Pearson's correlation metric on log-transformed values; genes detected in 10 cells or fewer were not considered in this analysis; where duplicate transcripts referred to the same gene, the transcript with the highest standard deviation was used to represent the gene.

Prostate organoid assay

Murine prostate epithelial cells were cultured with or without prostate stromal cells (1:2 ratio) in advanced DMEM/F12 supplemented with B27 (Life technologies, Grand Island, NY), 10 mM HEPES, Glutamax (Life technologies, Grand Island, NY), Penicillin/Streptomycin, and the following growth factors: EGF 50 ng/ml (Peprotech, Rocky Hill, NJ), 500 ng/ml recombinant R-spondin1 (Peprotech, Rocky Hill, NJ), 100 ng/ml recombinant Noggin (Peprotech, Rocky Hill, NJ), the TGF-β/Alk inhibitor A83-01 (Tocris, Ellisville, MO), and 10 μm Y-27632 (Tocris, Ellisville, MO). Dihydrotestosterone (Sigma, St. Louis, MO) was added to a final concentration of 1 nM. Cells are mixed with growth factor reduced Matrigel (Corning, Corning, NY) by 1:1 ratio and plated in 96-well plates. To determine the role of Wnt signaling, R-spondin was not added and 100 nM of IWP-2 (Selleck Chemicals, Houston, TX) was supplemented in the culture medium. To collect organoid for immunostaining, culture media were removed and 200 μl of 1 mg/mL Dispase solution (Invitrogen, Carlsbad, CA) was added and incubated for 1 hour at

37 °C. Samples were then transferred to 1.6 ml Eppendorf tubes and centrifuged at 900g for 2 minutes. Organoid were fixed in 10% formalin for 10 minutes and resuspended in 100 µl of HistoGel (Richard-Allan Scientific, Kalamazoo, MI) for preparation of paraffin embedded blocks.

To dissociate prostate organoids into single cells, organoids were released from Matrigel by Dispase (Life technologies, Grand Island, NY), resuspended in 300 µl of chilled Trypsin-Versene (Lonza, Walkersville, MD), and gently passed through 28-gauge insulin syringes for approximately 10 times in 5 minutes. 200 µl of organoid culture media was added followed by centrifuging at 900xg for 2 minutes. Dissociated cells were resuspended in culture media. Viable single cells were enumerated under microscope and plated in 96-well plates with growth factor reduced Matrigel (Corning, Corning, NY).

Prostate stromal cell culture

To determine how stable the molecular and phenotypic properties of the distinct prostate stromal subpopulations are, FACS-isolated subpopulations were either cultured in 2D in petridish with the organoid culture medium or suspended in growth factor reduced Matrigel (Corning, Corning, NY) and cultured in the organoid culture medium for 7-10 day. Outgrown cells were collected for subsequent qRT-PCR and flow cytometric analyses.

Histology and Immunostaining

Prostate tissues were fixed by 10% buffered formalin and paraffin embedded. HE staining and immunofluorescence staining were performed with 5 µm sections. To prepare cytospin from FACS-sorted cells, cells were loaded into cytospin slide chambers of Shannon Cytospin 4 (Thermal Scientific, Odessa, TX) and centrifuged at a speed of 800 rpm in room temperature for 5 minutes. H&E staining and immunofluorescence staining were performed using standard protocols on 5-µm paraffin sections or cytospin slides. Primary antibodies and dilutions used are listed below. Slides were incubated with 5% normal goat serum (Vector Labs, Burlingame, CA) and with primary antibodies diluted in 3% normal goat serum overnight at 4°C. Primary antibodies used in this study are rabbit anti-CD34 (ab81289, Abcam), rat anti-mouse CD90 (#105201, Biolegend), rat anti-Sca-1 (#557403, BD PharMingen, San Diego, CA) rabbit anti-K5

(#PRB-160P, Covance, Berkeley, CA), mouse anti-K8 (#MMS-162P, Covance), and mouse anti-K14 (sc-58724, Santa Cruz Biotechnology). Slides then were incubated with secondary antibodies (diluted 1:500 in PBST) labeled with Alexa Fluor 488 or 594 (Invitrogen/Molecular Probes, Eugene, OR). Sections were counterstained with 4,6-diamidino-2-phenylindole (DAPI) (Sigma-Aldrich, St. Louis, MO). Immuno-fluorescence staining was imaged using a Leica EL6000 confocal microscope (Leica Microsystems, Wetzlar, Germany).

STATISTICAL ANALYSES

All experiments were performed using 3-5 mice in independent experiments. Data are presented as mean ± s.d. or means ± SEM. Student's t test was used to determine significance between groups. For all statistical tests, the 0.05 level of confidence was accepted for statistical significance; more details are listed in figure legends.

DATA AVAILABILITY

The accession numbers for the single cell RNA-seq data is GEO: GSE119988. Detailed descriptions of data analysis and the software used can be found in Method Details.

SUPPLEMENTAL REFERENCE

Kwon, O.J., Zhang, L., Wang, J., Su, Q., Feng, Q., Zhang, X.H., Mani, S.A., Paulter, R., Creighton, C.J., Ittmann, M.M., *et al.* (2016). Notch promotes tumor metastasis in a prostate-specific Pten-null mouse model. The Journal of clinical investigation.
Valdez, J.M., Zhang, L., Su, Q., Dakhova, O., Zhang, Y., Shahi, P., Spencer, D.M., Creighton, C.J., Ittmann, M.M., and Xin, L. (2012). Notch and TGFbeta form a reciprocal positive regulatory loop that suppresses murine prostate basal stem/progenitor cell activity. Cell stem cell *11*, 676-688.